J|A|C|S
ARTICLES

Published on Web 05/12/2010

Single-Molecule Pulling Simulations Can Discern Active from Inactive Enzyme Inhibitors

Francesco Colizzi,*,† Remo Perozzo,‡ Leonardo Scapozza,‡ Maurizio Recanatini,† and Andrea Cavalli*,†,§

Department of Pharmaceutical Sciences, University of Bologna, Via Belmeloro 6, I-40126 Bologna, Italy, Pharmaceutical Biochemistry Group, School of Pharmaceutical Sciences, University of Geneva, Quai Ernest-Ansermet 30, CH-1211 Geneva 4, Switzerland, and Department of Drug Discovery and Development, Italian Institute of Technology, Via Morego 30, I-16163 Genova, Italy

Received January 11, 2010; E-mail: francesco.colizzi@unibo.it; andrea.cavalli@unibo.it

Abstract: Understanding ligand−protein recognition and interaction processes is of primary importance for structure-based drug design. Traditionally, several approaches combining docking and molecular dynamics (MD) simulations have been exploited to investigate the physicochemical properties of complexes of pharmaceutical interest. Even if the geometric properties of a modeled protein−ligand complex can be well predicted by computational methods, it is challenging to rank a series of analogues in a consistent fashion with biological data. In the unique β-hydroxyacyl-ACP dehydratase of *Plasmodium falciparum* (*Pf*FabZ), the application of standard molecular docking and MD simulations was partially sufficient to shed light on the activity of previously discovered inhibitors. Complementing docking results with atomistic simulations in the steered molecular dynamics (SMD) framework, we devised an *in silico* approach to study molecular interactions and to compare the binding characteristics of ligand analogues. We hypothesized an interaction model that both explained the biological activity of known ligands, and provided insight into designing novel enzyme inhibitors. Mimicking single-molecule pulling experiments, we used SMD-derived force profiles to discern active from inactive compounds for the first time. A new compound was designed and its biological activity toward the *Pf*FabZ enzyme predicted. Finally, the computational predictions were experimentally confirmed, highlighting the robustness of the drug design approach presented herein.

Introduction

Structure-based drug design approaches are increasingly used in hit identification, hit-to-lead, and lead optimization steps of the drug discovery process.[1−3] Molecular docking is a well-established structure-based approach, in which novel technological advances are constantly introduced to solve the multifaceted problem of ligand−receptor interaction.[4−7] Although brilliant strategies accounting for receptor flexibility are nowadays available,[8−10] the exhaustive and unbiased treatment of protein conformational changes upon ligand binding remains a major challenge. Moreover, the accurate prediction of relative or absolute ligand-binding affinities is an open long-standing question for docking algorithms.[11] Remarkable improvements have arisen from the development of combined protocols where docking outcomes are refined by means of physics-based simulation methods.[12−17] These approaches allow one both to account for the many degrees of freedom of the complex system, and to better estimate the ligand−protein binding free energy.[18] Although such advances have led to tremendous progress in protein−ligand recognition and interaction studies, it is only in a few cases that the computation of binding affinities has been prospectively exploited in lead discovery and optimization.[19,20]

† University of Bologna.
‡ University of Geneva.
§ Italian Institute of Technology.

(1) Bleicher, K. H.; Bohm, H. J.; Muller, K.; Alanine, A. I. *Nat. Rev. Drug Discovery* **2003**, *2* (5), 369–78.
(2) Jorgensen, W. L. *Science* **2004**, *303* (5665), 1813–8.
(3) Shoichet, B. K. *Nature* **2004**, *432* (7019), 862–5.
(4) Brooijmans, N.; Kuntz, I. D. *Annu. Rev. Biophys. Biomol. Struct.* **2003**, *32*, 335–73.
(5) Gohlke, H.; Klebe, G. *Angew. Chem., Int. Ed.* **2002**, *41* (15), 2644–76.
(6) Halperin, I.; Ma, B.; Wolfson, H.; Nussinov, R. *Proteins* **2002**, *47* (4), 409–43.
(7) Shoichet, B. K.; McGovern, S. L.; Wei, B.; Irwin, J. J. *Curr Opin Chem Biol* **2002**, *6* (4), 439–46.
(8) Bottegoni, G.; Kufareva, I.; Totrov, M.; Abagyan, R. *J. Comput.-Aided Mol. Des.* **2008**, *22* (5), 311–25.
(9) Bottegoni, G.; Kufareva, I.; Totrov, M.; Abagyan, R. *J. Med. Chem.* **2009**, *52* (2), 397–406.
(10) Totrov, M.; Abagyan, R. *Curr. Opin. Struct. Biol.* **2008**, *18* (2), 178–84.
(11) Leach, A. R.; Shoichet, B. K.; Peishoff, C. E. *J. Med. Chem.* **2006**, *49* (20), 5851–5.
(12) Deng, Y.; Roux, B. *J. Phys. Chem. B* **2009**, *113* (8), 2234–46.
(13) Gervasio, F. L.; Laio, A.; Parrinello, M. *J. Am. Chem. Soc.* **2005**, *127* (8), 2600–7.
(14) Huang, N.; Jacobson, M. P. *Curr. Opin. Drug Discovery Dev.* **2007**, *10* (3), 325–31.
(15) Jiao, D.; Golubkov, P. A.; Darden, T. A.; Ren, P. *Proc. Natl. Acad. Sci. U.S.A.* **2008**, *105* (17), 6290–5.
(16) Masetti, M.; Cavalli, A.; Recanatini, M.; Gervasio, F. L. *J. Phys. Chem. B* **2009**, *113* (14), 4807–16.
(17) Rastelli, G.; Del Rio, A.; Degliesposti, G.; Sgobba, M. *J. Comput. Chem.* **2010**, *31* (4), 797–810.
(18) Alonso, H.; Bliznyuk, A. A.; Gready, J. E. *Med. Res. Rev.* **2006**, *26* (5), 531–68.

Steered molecular dynamics (SMD) simulations have recently emerged as a flexible and powerful tool for providing information about the energy landscape driving ligand−receptor binding processes, and information about the time-resolved complex creation.[21] In the spirit of single-molecule experiments,[22] such as atomic force microscopy and laser optical tweezers,[23] SMD allows one to manipulate molecules to qualitatively probe mechanical functions in a versatile manner.[24] Additionally, quantitative estimates can be obtained if nonequilibrium descriptions for the analysis are employed.[25] Although widely used in studying ligand unbinding pathway and ligand−protein interactions, the ability of SMD simulations to characterize docking poses and to drive the selection of biologically active compounds (i.e., SMD as a drug discovery tool) has not yet been investigated, as far as we are aware. Here, we have tested the application of SMD simulations in the field of antimalarial drug discovery.

The high incidence of drug-resistant parasite strains and the lack of an effective vaccine means it is critical to develop antimalarial compounds.[26] *Plasmodium falciparum* (*Pf*) infections are estimated to be about half a billion annually. They continue to threaten lives as well as the economic development opportunities of countries in the tropical and subtropical zones of the world.[27,28] Malaria burden has stimulated investigators to search for novel target proteins and drug candidates. In recent years, the biosynthetic machinery involved in fatty acid production in Plasmodium has been regarded as a promising antimalarial target owing to the different structural organization of the enzymatic moieties between parasite and human.[29] Recently, independent studies have shown that parasitic fatty acid biosynthesis (FAS-II) plays a vital role in liver stage development and is not essential for the blood stages.[30,31] Moreover, using knockout parasites, Vaughan et al. have demonstrated that the lack of FAS-II renders the pre-erythrocytic parasite unable to successfully infect the mammalian host. In this scenario, FAS-II inhibitors could allow prophylactic strategies that would significantly contribute to malaria's eradication.[31]

In the elongation of the acyl chain in FAS-II, the growing acyl substrate is covalently bound to the acyl carrier protein (ACP), which shuttles and delivers the substrate from one enzyme to the other.[32,33] The unique β-hydroxyacyl-ACP dehydratase of *Pf* (*Pf*FabZ) catalyzes the dehydration of β-hydroxyacyl-ACP to form *trans*-2-enoyl-ACP. Its three-dimensional structure has been well-characterized by X-ray crystallography.[34,35] *Pf*FabZ's minimal structure is composed of a homodimer in which each monomer adopts the typical "hot dog" fold,[36] where six antiparallel β-sheets wrap around a long central α-helix (Figure 1). A certain proportion of structural plasticity has been observed in the region surrounding the active site, which occasionally bears unique structural properties among species.[37]

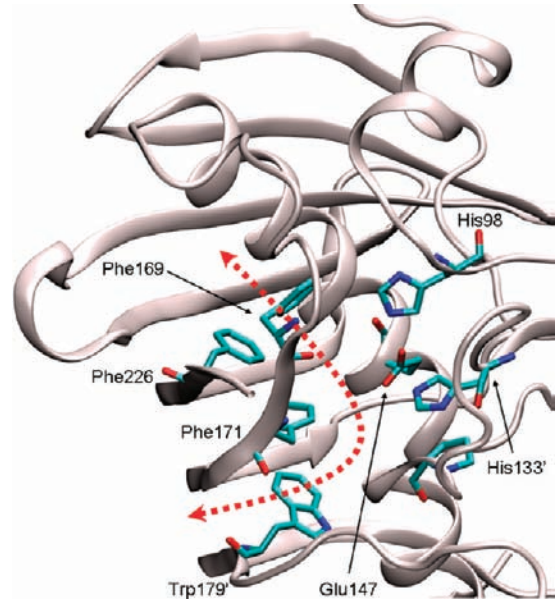

Figure 1. Close-up view of *Pf*FabZ's active site (carbon atoms in cyan sticks, pdbcode: 1Z6B). The dimer forms two independent L-shaped substrate binding tunnels with the catalytic sites at the interface (red dotted arrows, only one binding site is shown). The short segment of the L is the entrance tunnel that creates the access to the long tunnel segment by means of the gating Phe169 residue.[34,35] At the bottom of the entrance tunnel, there are three residues, the catalytic Glu147 and His133′ (from the other subunit), and His98, which represent the only hydrophilic spots in an overall hydrophobic substrate-binding site.

The literature does not yet include structure-based drug design studies that target *Pf*FabZ to produce novel antimalarial lead candidates. Nevertheless, recent studies have described both synthetic and natural compounds able to inhibit *Pf*FabZ's enzymatic activity.[38,39] In particular, Tasdemir et al.[38] have screened a large flavonoid library against *Pf*FabZ, finding competitive inhibitors showing mid- to low-micromolar activity.

In this paper, we describe a structure-based computational approach to studying molecular interactions and comparing the binding characteristics of ligand analogues *in silico*. In particular, we took advantage of the recently reported flavonoid *Pf*FabZ inhibitors, using a protocol that combines molecular docking and SMD simulations. We could thus characterize docking poses

(19) Jorgensen, W. L. *Acc. Chem. Res.* **2009**, *42* (6), 724–33.
(20) Kim, J. T.; Hamilton, A. D.; Bailey, C. M.; Domaoal, R. A.; Wang, L.; Anderson, K. S.; Jorgensen, W. L. *J. Am. Chem. Soc.* **2006**, *128* (48), 15372–3.
(21) Sotomayor, M.; Schulten, K. *Science* **2007**, *316* (5828), 1144–8.
(22) Deniz, A. A.; Mukhopadhyay, S.; Lemke, E. A. *J. R. Soc. Interface* **2008**, *5* (18), 15–45.
(23) Moffitt, J. R.; Chemla, Y. R.; Smith, S. B.; Bustamante, C. *Annu. Rev. Biochem.* **2008**, *77*, 205–28.
(24) Israelewitz, B.; Baudry, J.; Gullingsrud, J.; Kosztin, D.; Schulten, K. *J. Mol. Graphics Modell.* **2001**, *19* (1), 13–25.
(25) Liphardt, J.; Dumont, S.; Smith, S. B.; Tinoco, I., Jr.; Bustamante, C. *Science* **2002**, *296* (5574), 1832–5.
(26) Ting, L. M.; Gissot, M.; Coppi, A.; Sinnis, P.; Kim, K. *Nat. Med.* **2008**, *14* (9), 954–8.
(27) Sachs, J.; Malaney, P. *Nature* **2002**, *415* (6872), 680–5.
(28) Snow, R. W.; Guerra, C. A.; Noor, A. M.; Myint, H. Y.; Hay, S. I. *Nature* **2005**, *434* (7030), 214–7.
(29) White, S. W.; Zheng, J.; Zhang, Y. M. *Annu. Rev. Biochem.* **2005**, *74*, 791–831.
(30) Yu, M.; et al. *Cell Host Microbe* **2008**, *4* (6), 567–78.
(31) Vaughan, A. M.; O'Neill, M. T.; Tarun, A. S.; Camargo, N.; Phuong, T. M.; Aly, A. S.; Cowman, A. F.; Kappe, S. H. *Cell. Microbiol.* **2009**, *11* (3), 506–20.
(32) Byers, D. M.; Gong, H. *Biochem. Cell Biol.* **2007**, *85* (6), 649–62.
(33) Colizzi, F.; Recanatini, M.; Cavalli, A. *J. Chem. Inf. Model.* **2008**, *48* (12), 2289–93.
(34) Swarnamukhi, P. L.; Sharma, S. K.; Bajaj, P.; Surolia, N.; Surolia, A.; Suguna, K. *FEBS Lett.* **2006**, *580* (11), 2653–60.
(35) Kostrewa, D.; Winkler, F. K.; Folkers, G.; Scapozza, L.; Perozzo, R. *Protein Sci.* **2005**, *14* (6), 1570–80.
(36) Dillon, S. C.; Bateman, A. *BMC Bioinf.* **2004**, *5*, 109.
(37) Zhang, L.; Liu, W.; Hu, T.; Du, L.; Luo, C.; Chen, K.; Shen, X.; Jiang, H. *J. Biol. Chem.* **2008**, *283* (9), 5370–9.
(38) Tasdemir, D.; Lack, G.; Brun, R.; Ruedi, P.; Scapozza, L.; Perozzo, R. *J. Med. Chem.* **2006**, *49* (11), 3345–53.
(39) Sharma, S. K.; Kapoor, M.; Ramya, T. N.; Kumar, S.; Kumar, G.; Modak, R.; Sharma, S.; Surolia, N.; Surolia, A. *J. Biol. Chem.* **2003**, *278* (46), 45661–71.

Chart 1. Chemical Structures of the Flavonoid Lead Compound Luteolin (IC_{50} = 5 μM)[a] and of Some Representative Analogues

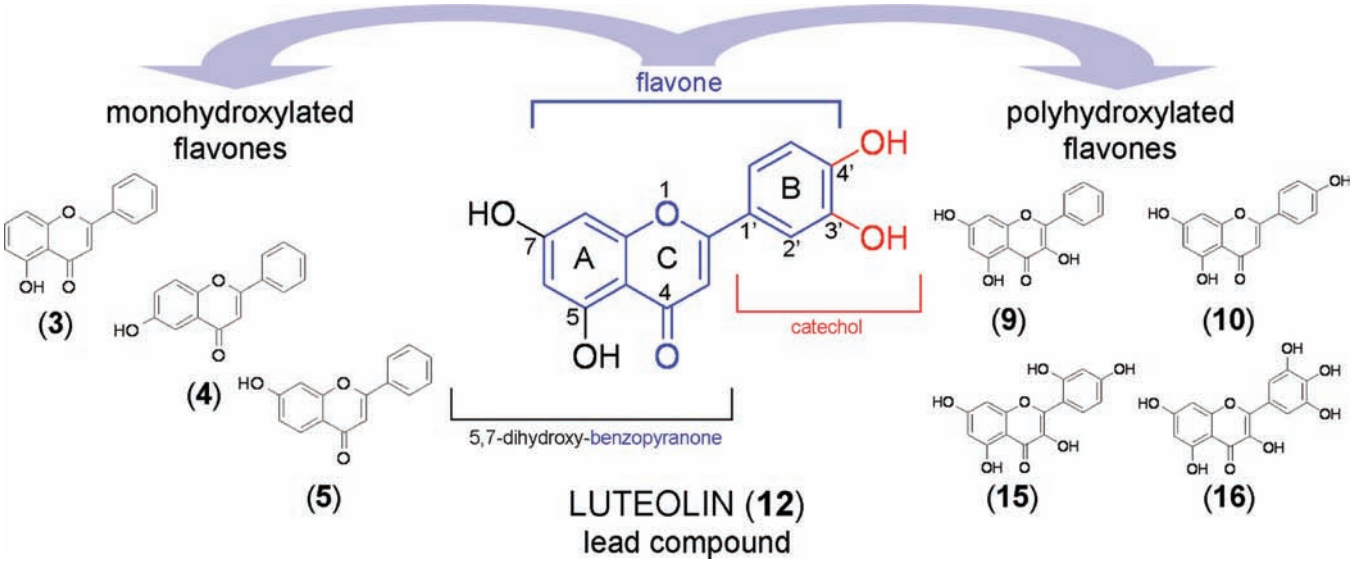

[a] Inhibition data against *Pf*FabZ and compound number are taken from Tasdemir et al.[38]

and discern active from inactive flavonoids by simply analyzing the SMD-derived force profiles related to ligand unbinding simulations. Moreover, the presented approach allowed us to rationalize the structure−activity relationship (SAR) of the flavonoid series, and, finally, to design and predict the biological activity of a novel *Pf*FabZ inhibitor. Subsequent experimental assays validated the accuracy of our approach.

Results and Discussion

SMD Toolbox: Motivation and General Strategy. Herein, we rationalize the biological activity of flavonoids (Chart 1) against *Pf*FabZ by combining docking with SMD simulations, which could provide essential information on the ligand−protein complex dynamics. First, docking studies were carried out to investigate the flavonoid−*Pf*FabZ interactions for the series of monohydroxylated derivatives (**3**−**5** in Chart 1). The position of the hydroxy substituent crucially influenced inhibitory activity against *Pf*FabZ. The biological data showed that 6- and 7-hydroxy substituted (**4** and **5**) derivatives were active, while the introduction of a hydroxyl group in 5- (**3**) led to an inactive compound.[38] A possible explanation was provided by analyzing the docking outcomes shown in Figure 2. The compounds docked at the substrate entrance-tunnel, sharing a similar interaction pattern between the carbonyl group of flavone and the backbone of Val143′ (dotted black line in Figure 2A). While the 6-hydroxy derivative interacted with the side chains of Glu147 and His98, 7-hydroxy flavone established H-bond interactions with the side chain of His98 and the backbone of Phe169. Conversely, the 5-hydroxy analogue suffered from relevant steric clashes with Glu147 (dotted purple curves in Figure 2A). This repulsion was accounted for by the scoring function, and its nature was well-described by the H-bond and steric-clash scoring terms (Figure 2B). As a consequence, the inactive 5-hydroxy flavone obtained a lower overall score (red plot, Figure 2B) when compared to the active 6- and 7-hydroxy analogues.

Molecular docking allowed a straight rationalization of biological data for the monohydroxylated flavones. However, it was unable to discern active from inactive compounds for

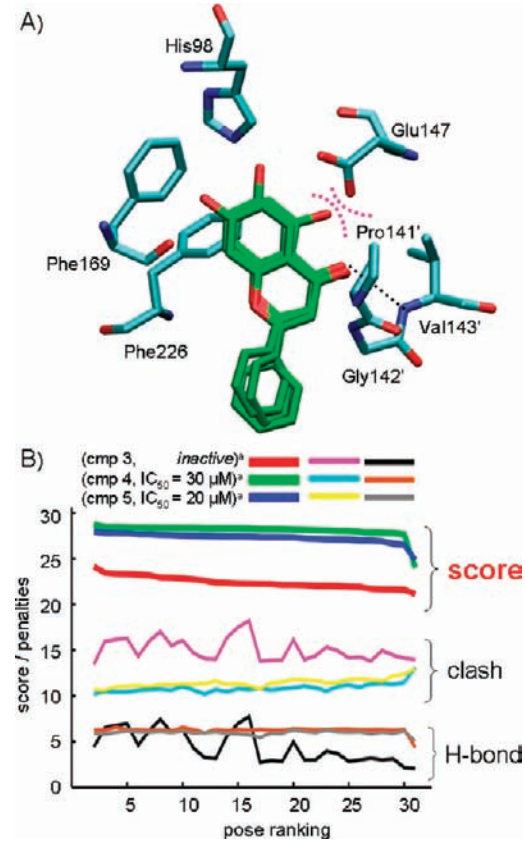

Figure 2. Molecular docking outcomes for monohydroxylated flavones. (A) Binding mode of 5-, 6-, and 7-hydroxyflavone (**3**, **4**, **5**; carbon atoms in green) docked into the catalytic pocket of *Pf*FabZ. The purple dotted curves highlight the steric clashes between Glu147 and the 5-OH of **3**. For each ligand, the representative pose of the most populated cluster is shown. (B) Representation of the scoring function trend over 30 docked poses. The concerted behavior of the H-bond (black) and steric-clash (pink) terms for **3** reflects the unfeasible combination of favorable H-bond interactions at low clash-penalty costs. [a]Inhibition data against *Pf*FabZ are taken from Tasdemir et al.[38]

the polyhydroxylated derivatives (Chart 1). The biological data of polyhydroxylated flavones could not be rationalized by analyzing docking outcomes in terms of scoring, geometry, and pose population. This probably reflects the ability of these derivatives to interact with the biological counterpart in different and energetically degenerate ways.[40] Furthermore, experimental data have suggested structural plasticity as a peculiar feature of *Pf*FabZ.[34,35] In this light, even small changes in the receptor conformation could dramatically affect the final docking outcome. The application of various consensus docking or scoring schemes might often overcome the limitation of single-pose scoring or sampling methods.[41−43] However, MD-based approaches are also able to capture critical structural rearrangements, which the biological system may experience upon ligand-binding (i.e., induced fit or population shift).[29,32] In this respect, molecular docking can be used to rapidly explore the ligand−receptor configurational space, providing MD simulations with reliable starting configurations, which are then evolved along nanosecond-scale trajectories and eventually used for estimating ligand−receptor binding affinities.[14,16,18] Since the ligand−receptor binding/unbinding event is rarely sampled by nanosecond-time-scale MD simulations, we used SMD to study the energetics of the time-resolved complex formation. SMD allows us to apply a time-dependent external force to encourage the system to evolve along a predefined reaction coordinate. In unbinding simulations, SMD is exploited to pull the ligand out of the protein, thus, sampling the major ligand−protein interaction coordinate. Since the ligand is harmonically restrained to a constant-velocity moving point, it is possible to obtain the mechanical irreversible work necessary for the undocking by integrating the force exerted on the system along the unbinding reaction coordinate. Furthermore, by a repeated sampling of the biased unbinding trajectory, the Jarzynski nonequilibrium work theorem[44] can be exploited to discount the dissipated work, and to reconstruct the potential of mean force (PMF) profile along the selected reaction coordinate.[45−47]

To study the molecular interactions involved in the ligand−protein (e.g., flavonoid−*Pf*FabZ) complex formation, we devised a broadly applicable SMD toolbox by combining docking and SMD simulations. The general protocol is outlined in Scheme 1 and relies on two subsequent steps: (1) the binding mode of the lead compound is predicted by providing a rather detailed energetic evaluation of ligand−protein binding using Jarzynski-equation-based methods;[45,48] (2) using the binding mode of the lead as a reference, the bioactivity of related compounds against the target is probed and predicted by reiterating fast SMD undocking runs. The SMD toolbox was applied to investigate the binding properties of polyhydroxylated flavones against *Pf*FabZ using luteolin (**12**) as reference lead compound. Employing the outcomes of steps (1) and (2), we were able to

Scheme 1. The SMD Toolbox Flowchart[a]

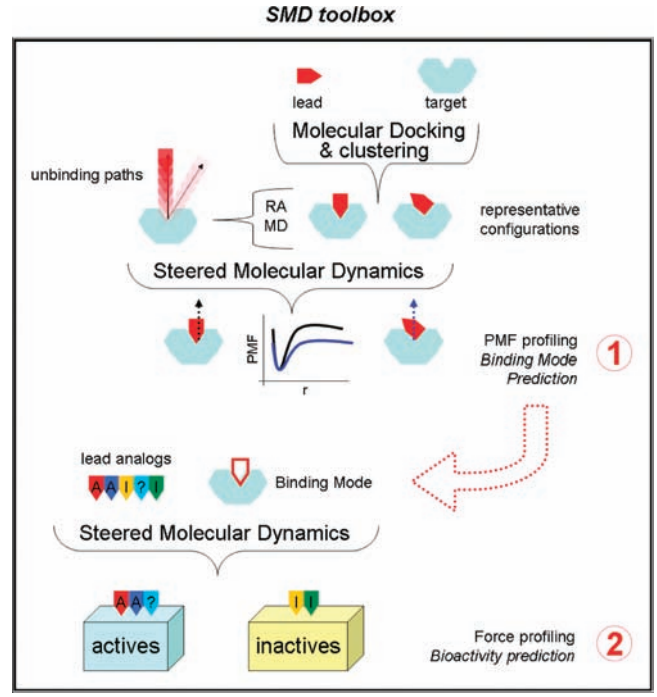

[a] The unbinding paths were investigated using Random Acceleration MD (RAMD, see the Computational Methods for further details).

both rationalize the biological data of *Pf*FabZ ligands, and assist in the design of novel inhibitors.

1. Luteolin Binding to *Pf*FabZ. Docking poses of **12** at the binding site of *Pf*FabZ were generated using a genetic algorithm, which provided a population of ligand configurations at the receptor binding site.[49] The outcomes were then processed by a hierarchical-agglomerative clustering procedure, which has been proven to efficiently reduce the dimensionality of the original data set and to highlight the most relevant docking poses.[41,50] We obtained two clusters of docking configurations: one significantly populated according to the Chauvenet criterion,[41] and the other less populated but containing the best ranked docking pose (according to GOLD scoring functions).[49] The representative pose for each of the two clusters, which covered together more than 90% of the sampled configurational space, was subsequently submitted to MD simulations.

The two resulting binding modes of **12**, corresponding to the best ranked docking pose and to the most populated one (hereafter referred to as **12-A** and **12-B**, respectively) are shown in Figure 3.

In both models, luteolin was embedded in the same region of the binding site occupying the entrance of the tunnel, and being in close proximity to the catalytically relevant residues Glu147, His133′, and of His98. In configuration **12-A**, the catechol ring was buried, while in **12-B** it was more solvent-exposed. In detail, **12-A** showed the catechol moiety pointing deep into the binding pocket, and its hydroxyl groups in positions 3′ and 4′ established H-bond interactions with Glu147, His133′, and His98 side chains, and Phe169 backbone (Figure 3A). During MD simulations, the triad of phenylalanines (Phe169, Phe171, and Phe226) reshaped the binding cavity and

(40) Zhang, L.; Kong, Y.; Wu, D.; Zhang, H.; Wu, J.; Chen, J.; Ding, J.; Hu, L.; Jiang, H.; Shen, X. *Protein Sci.* **2008**, *17* (11), 1971–8.
(41) Bottegoni, G.; Rocchia, W.; Recanatini, M.; Cavalli, A. *Bioinformatics* **2006**, *22* (14), e58–65.
(42) Charifson, P. S.; Corkery, J. J.; Murcko, M. A.; Walters, W. P. *J. Med. Chem.* **1999**, *42* (25), 5100–9.
(43) Paul, N.; Rognan, D. *Proteins* **2002**, *47* (4), 521–33.
(44) Jarzynski, C. *Phys. Rev. E: Stat., Nonlinear, Soft Matter Phys.* **2006**, *73* (4 Pt 2), 046105.
(45) Jensen, M. O.; Park, S.; Tajkhorshid, E.; Schulten, K. *Proc. Natl. Acad. Sci. U.S.A.* **2002**, *99* (10), 6731–6.
(46) Minh, D. D.; McCammon, J. A. *J. Phys. Chem. B* **2008**, *112* (19), 5892–7.
(47) Park, S.; Schulten, K. *J. Chem. Phys.* **2004**, *120* (13), 5946–61.
(48) Jarzynski, C. *Phys. Rev. Lett.* **1997**, *78* (14), 2690–3.
(49) Jones, G.; Willett, P.; Glen, R. C.; Leach, A. R.; Taylor, R. *J. Mol. Biol.* **1997**, *267* (3), 727–48.
(50) Bottegoni, G.; Cavalli, A.; Recanatini, M. *J. Chem. Inf. Model.* **2006**, *46* (2), 852–62.

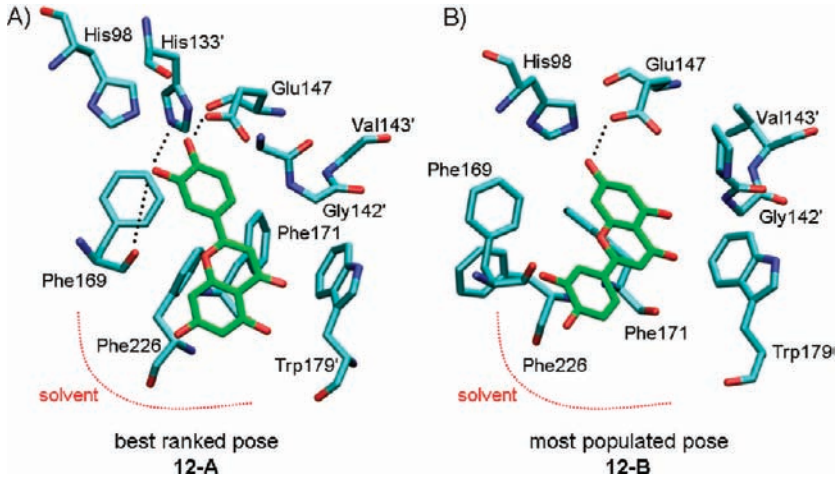

Figure 3. Luteolin (carbon atom in green) interacting with *Pf*FabZ active site. Docking poses after 3 ns of MD simulations. Molecular details of the binding modes corresponding to, (A) the best ranked docking pose, and (B) the most populated one (His133′ was not displayed for the sake of clarity). Dotted black lines stand for H-bond interactions. Note the different ensemble of conformations assumed by the triad of phenylalanines (Phe169, Phe171, and Phe226).

allowed for the favorable docking of the flavonoid core. The 5-OH and 7-OH were particularly exposed to the solvent bulk and the remaining polar groups of the ligand were poorly involved in interactions with the protein. In configuration **12-A**, the catechol ring was involved in several interactions with the enzyme's active site. In contrast, the catechol moiety scarcely interacted with the protein in **12-B** (Figure 3B). Here, the benzopyranone core was embedded in the binding pocket with only the 7-OH able to establish H-bond interactions with Glu147, while the rest of the ligand populated several docking configurations.

In Figure 4A, the root-mean-square deviations (rmsd) of **12-A** and **12-B** versus simulation time are shown.

The stable evolution of **12-A** (Figure 4A, red plot) suggested the presence of a narrow energy well for this pose. Vice versa, **12-B** (Figure 4A, green plot) showed a less stable evolution, probably because it belonged to a wider energy well in which several local minima were separated by k_BT energy barriers, and therefore accessible by nanosecond-time-scale simulations (Figure 4B). Such behavior was consistent with the fact that the starting configuration of **12-B** belonged to the most-populated cluster.[51] Furthermore, these results could reflect a greater enthalpic contribution for **12-A**, while the higher number of configurations available for **12-B** could account for an entropic stabilization. Entropy could stabilize **12-B** at higher energy regions of the energy hypersurface.[52] Remarkably, entropy is generally poorly accounted for by routinely used docking scoring functions. Cluster analysis could help to roughly estimate the entropic contribution by determining whether or not a pose belongs to a widely populated group of docking configurations.[51,53,54] However, such an approach is a long way off from quantitatively accounting for the entropic contribution to the ligand−protein interaction.

To univocally establish the more favored binding mode (between **12-A** and **12-B**), we carried out undocking experiments by using constant-velocity SMD (Figure 5). The PMF

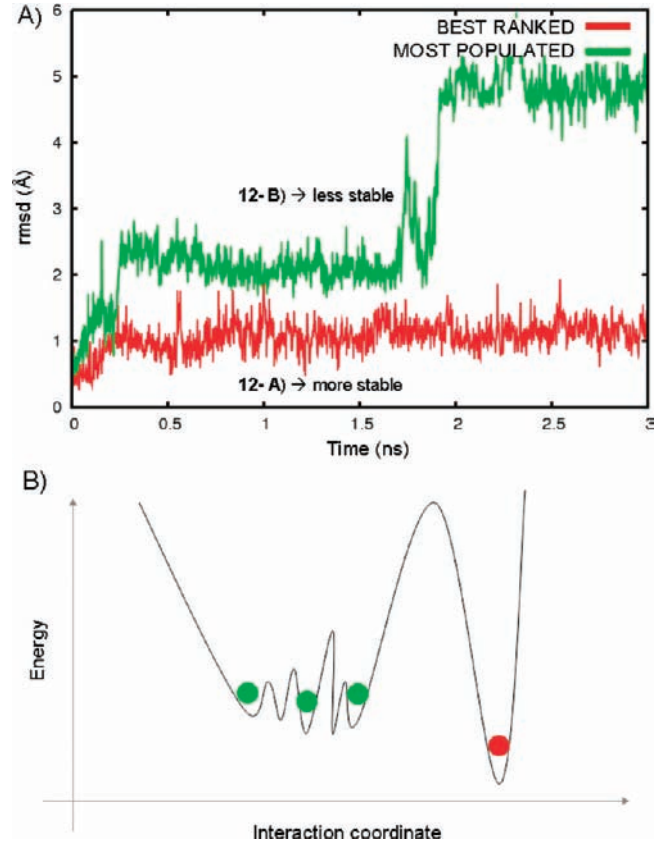

Figure 4. Qualitative differences between the best ranked **12-A** (red) and most populated **12-B** (green) docking poses. (A) Root mean square deviation (rmsd) of the thermalized docking poses along 3 ns of unrestrained MD trajectory. (B) Schematic representation of the energy profile along an arbitrarily chosen interaction coordinate. The most populated pose (green) likely belongs to a wider energy basin, in which similar configurations can easily interchange among one another. The best ranked pose (red) falls into a narrow minimum and interchanges poorly.

of the *Pf*FabZ−luteolin unbinding process was thus reconstructed, pointing to the more stable pose in terms of free energy (Figure 6).

The profiles of the force exerted on the system to encourage the undocking of **12-A** and **12-B** along a carefully predefined

(51) Kozakov, D.; Schueler-Furman, O.; Vajda, S. *Proteins* **2008**, *72* (3), 993–1004.
(52) van Gunsteren, W. F.; et al. *Angew. Chem., Int. Ed.* **2006**, *45* (25), 4064–92.
(53) Xiang, Z.; Soto, C. S.; Honig, B. *Proc. Natl. Acad. Sci. U.S.A.* **2002**, *99* (11), 7432–7.
(54) Lee, J.; Seok, C. *Proteins* **2008**, *70* (3), 1074–83.

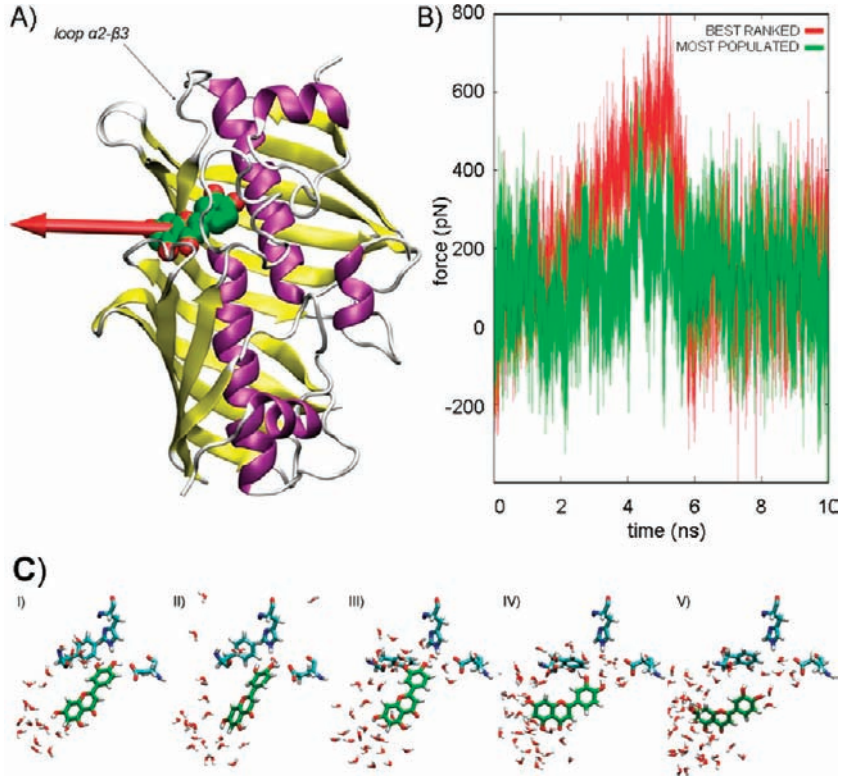

Figure 5. Pulling luteolin out of the *Pf*FabZ binding pocket. (A) The red thick arrow represents the pulling direction for the ligand unbinding pathway. (B) Typical profiles of the force exerted on luteolin to induce the unbinding of the best ranked **12-A** (red plot) and the most populated **12-B** (green plot) docking configurations. (C) Water molecules assisting the rupture of the anchoring interaction between luteolin (carbon atoms in green) and *Pf*FabZ (carbon atoms in cyan). Snapshot isolated from the unbinding of **12-A** at different undocking levels from (I) the initial bound state to the (V) almost fully solvated ligand. The rupture event occurred between (III) and (IV).

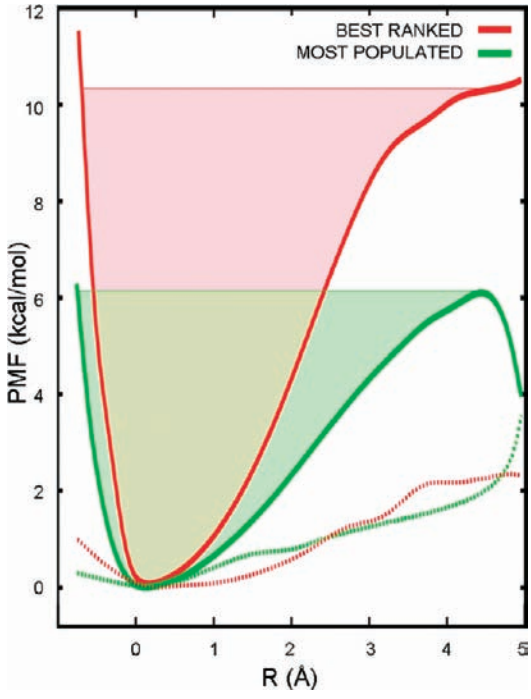

Figure 6. Potential of mean force (PMF) along the unbinding reaction coordinate. The reaction coordinate (R) was defined as the distance of the center of mass of luteolin from the equilibrated docking configuration along the pulling direction shown in Figure 5. The free energy profiles (PMF) (solid lines) of the best ranked (red, **12-A**) and the most populated (green, **12-B**) poses are compared. The dotted lines represent the corresponding dissipated work calculated from $\sigma_w^2/2k_BT$. The normalized values of the surfaces subtended by the PMF plots were 1 for **12-A** and 0.6 for **12-B**.

reaction coordinate (Figure 5A, see also section Computational Methods for further details) are shown in Figure 5B. Notably, during the undocking of **12-A**, the force magnitude reached a value of ∼600 pN, while a much flatter force profile was observed (∼300 pN) for **12-B**. The force profiles correlated well with the rupture of the anchoring interactions (mainly H-bonds) between luteolin and *Pf*FabZ. In particular, the undocking was controlled by a breakup in the charge-reinforced H-bond interaction network between ligand hydroxyl group(s) and Glu147 side chain. This observation was extremely informative since it pointed out the crucial role of this network in anchoring the ligand to its target protein. Relating the drops in the force profiles with the undocking trajectories, it was possible to infer the critical role played by the catechol ring in anchoring configuration **12-A** at the enzyme active site. The extremely slow pulling velocity of 0.5 Å/ns minimized the friction influence on the unbinding process, and could allow water molecules to solvate the interacting counterparts, and assist the breaking of the interactions at a lower energetic cost (Figure 5C).

The second order cumulant expansion of the Jarzynski Equality (see Experimental Procedures, eq 2) was then used to reconstruct the PMF from reiterated SMD trajectories collected along the undocking of **12-A** and **12-B** (Figure 6, red and green plot, respectively). The PMF profiles corresponding to the rupture of the anchoring interactions during the unbinding event differed in both basin width and well depth. Consistently with docking results, the narrow energy basin found for **12-A** could be related to the lower population of the best scored docking configuration. Similarly, **12-B** was found to belong to a wider energy basin, likely reflecting the broader region of ligand

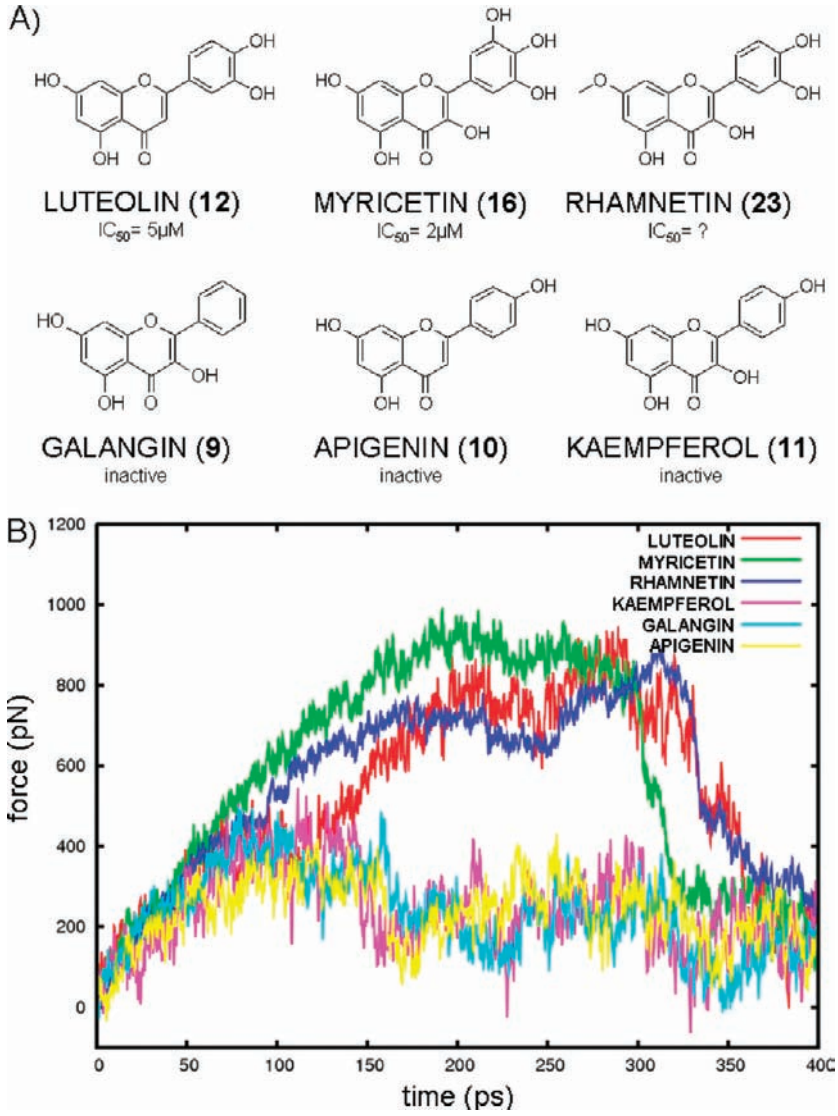

Figure 7. Comparison of the undocking force profiles of different flavonoid ligands. (A) Chemical structures of ligands under investigation. Inhibition data against *Pf*FabZ are taken from Tasdemir et al.[38] (B) Force profiles deriving from pulling the ligands along the unbinding reaction coordinate. For each ligand, the plots show the resulting mean values from averaging the force profiles from five different SMD runs.

attraction, which is commonly associated with highly populated poses.[51,54] The PMF also provided an indication of the free energy well depth associated with **12-A** and **12-B**. The unbinding of **12-A** needed to overcome an energy barrier of ∼9 kcal/mol, while **12-B** met an unbinding energy barrier of ∼5 kcal/mol. While the calculation of absolute binding free energy is out of the scope of this investigation, it should be acknowledged that highly accurate estimation of binding constants is not always essential for productive studies in drug design. For instance, the SMD-based PMF could be successfully exploited as a quantitative tool to assess different modes of binding. Here, the **12-A**/**12-B** relative population could be roughly estimated by the ratio between the surfaces subtended by the corresponding PMF plots, and one might reasonably infer that **12-A** is the most thermodynamically stable configuration for the luteolin−*Pf*FabZ complex.

2. Inhibitor Design and Relative Affinity Prediction. Having established that **12-A** represents the preferred binding mode of luteolin, we then evaluated whether this conclusion could be exploited to rationalize and predict the biological activity of representative flavonoid analogues reported in Figure 7A. According to the unbinding of configuration **12-A**, one might infer that polyhydroxylated flavonoids require two or more hydroxyl groups in the B ring to allow for a productive binding to *Pf*FabZ. Indeed, our undocking simulations showed that in **12-A**, the catechol B ring primarily anchored the ligand into the pocket, and that the substituent at position 7 in the benzopyranone core played a noncritical role in the unbinding process. In fact, in **12-A**, the 7-OH was not directly involved in any interaction with the enzyme, suggesting that a bulkier substituent could be able to maintain the inhibitory activity. These observations were in very good agreement with the experimental data reported by Tasdemir et al.[38] (Figure 7). To definitively assess the robustness of the SMD toolbox in computational drug design, we predicted the biological activity of a new and previously unreported flavonoid derivative as *Pf*FabZ inhibitor. A new molecule (rhamnetin, **23**) was designed by substituting the 7-OH of **11** (kaempferol) with a 7-OMe and by inserting on the same molecule a second OH group in position 3′ of the B ring (Figure 8). Figure 7A shows the chemical structure of two active, luteolin, myricetin (**12**, **16**) and three inactive compounds, galangin, apigenin and kaempfer-

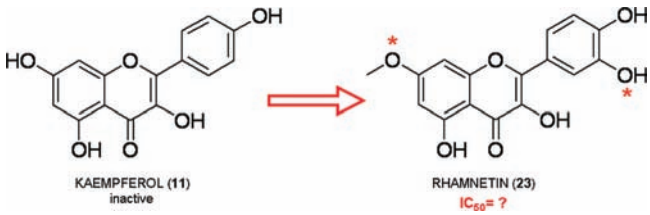

Figure 8. Structure-based ligand design. The red stars highlight the newly introduced functional groups. Note the presence of at least two OH in the B-ring and the 7-OMe substitution.

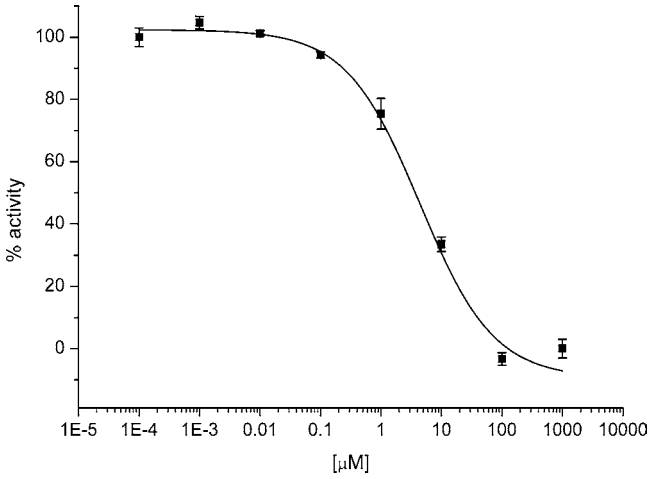

Figure 9. Inhibition of *Pf*FabZ by rhamnetin at increasing concentrations of the inhibitor. The enzyme activity is reduced by 50% at an inhibitor concentration of 4.4 μM.

ol (**9**−**11**), which were computationally investigated along with the novel molecule, rhamnetin (**23**) (in Figure 7B, the undocking force profiles are reported; see below). The relative binding affinity of **23** was predicted by SMD simulations. For each ligand−protein complex, an external force was applied to the ligand to steer it along the unbinding reaction coordinate. The exerted forces could be monitored throughout the entire simulation. Two major scenarios were observed (Figure 7B): one related to the unbinding of active ligands, and the other corresponding to inactive flavonoids. The unbinding of each of the inactive compounds was induced by a force not higher than ~400 pN, while active compounds required an unbinding force of ~800 pN. The analysis of the force profiles plotted in Figure 7B shows how the novel compound rhamnetin (blue plot) clearly grouped with the micromolar inhibitors, thus, predicting its binding affinity toward *Pf*FabZ in the micromolar range.

The inhibitory activity of rhamnetin against the purified *Pf*FabZ enzyme was then experimentally determined. As shown in Figure 9, the IC_{50} value for rhamnetin was 4.4 μM, very similar to those of luteolin and myricetin, 5 and 2 μM, respectively. This result falls nicely in the range of actives, validating both the design strategy and the binding hypothesis for the flavonoid−*Pf*FabZ interaction. To the best of our knowledge, this is the first report on a straightforward exploitation of SMD in drug design.

In light of the SMD results, we could further comment on the SAR of the present series of *Pf*FabZ inhibitors. The inactive compound **9** (galangin), which does not bear hydroxyl groups on the B ring, could not establish a proper H-bond interaction network with the enzyme active site, and its undocking force profile was rather flat. Adding only one hydroxyl group on the flavone B ring was still not enough to establish a proper network of H-bond interactions. As a consequence, **10** (apigenin) did not show a significant inhibitory activity, and its force profile was rather flat (Figure 7B). In contrast, the 3′-OH and 4′-OH of **12** (luteolin) could properly establish the H-bond interactions with *Pf*FabZ catalytic residues responsible for the higher magnitude of the force observed in Figure 7B. Interestingly, the biological activity is not related to the 3′-OH itself, as demonstrated by the *Pf*FabZ inhibitory activity of **15** (morin, $IC_{50} = 8$ μM,[38] Chart 1) which bears two hydroxyl groups on the B ring in position 2′ and 4′. We could therefore conclude that (at least) two OH groups on the B ring are strictly required to establish a proper binding of polyhydroxylated flavonoids to *Pf*FabZ.

Although it would be unwise to relate the slightly different biological activities of luteolin, myricetin, and rhamnetin, to the slightly different magnitudes of their force profiles, it is interesting to note how inactive compounds were characterized by very similar force profiles. Conceivably, this was due to the computational approach's ability to capture dynamic physicochemical properties of the interactions, which are generally missed in a static view of the binding event. While we do not consider the protocol (in its present state) to be a means for accurate binding affinity prediction, the possibility of using the SMD-based procedure to discriminate binders from nonbinders in a rough and fast way clearly emerges. Two major scenarios can be observed: (i) when the pulled ligand can easily advance along the selected reaction coordinate, the applied force is small and its profile rather flat (inactive compound); (ii) conversely, if the ligand is more tightly bound to its receptor (active compound) and encounters more resistance during the unbinding, the applied force increases to overcome energy barriers, thus, resulting in quite relevant drops in the force profile. In this respect, when small modifications are present on a common ligand scaffold and receptor conformational changes are neglected upon ligand−protein binding, docking methods might be unable to properly rank different series of analogues. In contrast, here we have demonstrated that SMD could be applied efficiently to properly discriminate actives from inactives within a series of compounds, and to explicitly account for protein flexibility upon ligand (un)binding.

Conclusions

We have reported for the first time on the possible exploitation of a combined computational protocol (SMD toolbox) based on docking, cluster analysis, and SMD simulations to study molecular interactions and compare the binding characteristics of ligand analogues *in silico*.

From a computational drug discovery perspective, our protocol could efficiently complement routinely applied docking simulations, especially when small structural modifications are present on a series of analogues. Indeed, in these situations, docking studies often fail to properly rank the binding affinities, particularly when the receptor is treated rigidly. SMD force profiles of fully solvated ligand−protein complexes could offer a way to face some of the major drawbacks of the currently applied structure-based approaches. Further tuning of the SMD toolbox might allow researchers to not only discern actives from inactives, but also prioritize active ligands based on their relative affinity toward the biological target under investigation. Moreover, once the unbinding trajectories are generated, deriving the force profile is straightforward and data processing can be easily automated.

This study lays down the basis for the development of a new structure-based ligand discovery tool, which could be used to reconstruct the ligand−target binding event at the atomistic level in a fully solvated and flexible manner, and at a reasonable computational cost.

Experimental Procedures

1. Computational Methods. 1.1. Docking Model Building. The initial 3D coordinates of *Pf*FabZ were retrieved from the Protein Data Bank (apo structure; pdb code: 1z6b). Chains A and B were selected to simulate the protein dimer and the disordered portions were rebuilt using standard parameters of the loop modeling routine implemented in MODELLER 7.0.[55] The structure of flavonoid ligands was built and geometry optimized using the molecular modeling suite of programs Sybyl 7.3 (Tripos, Inc., St. Louis, MO). Molecular Docking was carried out using the default setting parameters of Gold 3.0.1.[49] The binding site definition included the γC of Phe169 chain A and every residue within 15 Å. For the 5-, 6-, and 7-hydroxyflavone series, ChemScore was used to drive and rank the genetic algorithm search. The preliminary docking calculations on the polyhydroxylated flavonoid series were performed using both GoldScore and ChemScore. Docking poses for luteolin were obtained using both GoldScore and ChemScore and 100 poses were generated with each scoring function. Docking outcomes were then submitted to cluster analysis by means of the AClAP program,[41,50] and only one significantly populated cluster was obtained (cardinality of 153). According to the Chauvenet criterion implemented in AClAP, a cluster is significantly populated when its cardinality is more than twice the standard deviation apart from the average population value for that level of clustering. The second most populated cluster (cardinality of 33) was the one containing the best ranked pose of luteolin.

1.2. Molecular Dynamics Simulations. Luteolin (**12**) was used as a reference compound for setting up the SMD toolbox. The representative pose (chosen as the closest conformation to the cluster centroid) for each of the two most populated clusters was selected and each ligand−protein complex (**12-A** and **12-B**) was further investigated by means of MD as described below. The complex was solvated with an 8 Å thick layer of water using the solvatebox command of the LEaP program[56] and the electroneutrality was imposed by equally distributing the excess total charge (+6) over the 4656 atoms of the protein. Periodic boundary conditions were applied and long-range electrostatic interactions were calculated every time step by using the Particle Mesh Ewald (PME) method.[57] A cutoff of 10 Å was used for van der Waals and short-range electrostatic interactions with a smoothing switching function starting at 8 Å. Time integration step of 2 fs was used and the length of all bonds involving hydrogen atoms was constrained using the SHAKE algorithm.[58] The solvated system was minimized for 1000 steps restraining the heavy atoms, except waters, with a force constant of 5 kcal mol^{-1} Å^{-2}, followed by 1000 steps with a force constant of 3 kcal mol^{-1} Å^{-2} applied to the backbone and finally minimizing the unrestrained system for a further 1000 steps. At constant volume (NVT ensemble), the system was heated from 1 up to 300 K by increments of 50 K every 15 ps and, correspondingly, the α-carbons were gradually unrestrained by lowering the spring constant from 6 to 2 kcal mol^{-1} Å^{-2}. The temperature was controlled by the Langevin thermostat with a dumping coefficient of 5 ps^{-1}. During the subsequent switching to the isothermal−isobaric (NPT) ensemble, a soft harmonic restraint of 1 kcal mol^{-1} Å^{-2} was still applied to the Cα atoms and gradually turned off in the next 60 ps. The Langevin piston method was used to set the target pressure at 1 atm. The system evolved for a further 3 ns and the starting configurations for both unbinding pathway investigation and SMD simulations were randomly sampled from the last 300 ps. All simulations were performed with NAMD 2.6[59] using the AMBER99SB force field[60] for protein and the TIP3P model for all water in the system.[61] The flavonoid ligands were optimized using the Gussian03 software (Gaussian, Inc. Wallingford, CT) at the HF/6-31G* level of theory and partial atomic charges were assigned using the restricted electrostatic potential fit (RESP) method.[62] The general AMBER force field (GAFF)[63] was used for the ligands and the corresponding topology and parameters files were prepared with the antechamber tool of the AMBER suite of programs.[56]

1.3. Ligand Unbinding Reaction Coordinate. A few strategies have been used to determine the direction of the biasing potential in single-molecule pulling simulations. The most widely used approach, especially for studying mechanical functions of macromolecules, is based on structural information.[24,64] Conversely, physics-based methods, such as Locally Enhanced Sampling (LES)[65] and, more recently, Random Acceleration/Expulsion Molecular Dynamics (RAMD),[66] have been successfully used to disclose putative ligand unbinding pathways in biologically relevant targets.[67−71] The unbinding reaction coordinate was here investigated using the RAMD approach introduced by Luedemann et al.[66] This method offers at least two unique advantages in the SMD framework: (i) low computational cost, and (ii) objective pathway search. Hence, an unbiased search for ligand escape pathways was pursued by reiterating individual MD simulations in which a randomly oriented force was applied to the ligand in addition to the standard force field. A randomly oriented force is applied to the ligand atoms for a defined short amount of time-steps *N*. The force has constant magnitude *f* and accelerates the ligand in the context of the binding pocket. If the ligand encounters hindrance during the route, its average velocity will fall below a preset threshold or, in other words, it will not cover the expected distance r_{min} in the *N* time steps. If this is the case, a new direction is chosen randomly and maintained for a further *N* steps, as long as the ligand finds a path which allows the coverage of the r_{min} distance. The probability of sampling the unbinding event depends on the system's structural peculiarities, on the type of interactions involved in the ligand−protein complex, and on the combination of the adjustable parameters *f*, *N*, and r_{min}.[68,69] For the luteolin−*Pf*FabZ complex, three combinations of parameters were tested, finding an expulsion rate ranging from 3% to 41% (see Table 1). For each combination, 100 independent trajectories were generated. If no expulsion was

(55) Fiser, A.; Do, R. K.; Sali, A. *Protein Sci.* **2000**, *9* (9), 1753–73.
(56) Case, D. A.; et al. *AMBER 9*; University of California: San Francisco, CA, 2006.
(57) Darden, T.; York, D.; Pedersen, L. *J. Chem. Phys.* **1993**, *98* (12), 10089–92.
(58) Ryckaert, L. P.; Ciccotti, G.; Berendsen, H. J. C. *J. Comput. Phys.* **1977**, *23*, 327–341.
(59) Phillips, J. C.; Braun, R.; Wang, W.; Gumbart, J.; Tajkhorshid, E.; Villa, E.; Chipot, C.; Skeel, R. D.; Kale, L.; Schulten, K. *J. Comput. Chem.* **2005**, *26* (16), 1781–802.
(60) Hornak, V.; Abel, R.; Okur, A.; Strockbine, B.; Roitberg, A.; Simmerling, C. *Proteins* **2006**, *65* (3), 712–25.
(61) Jorgensen, W. L.; Chandrasekhar, J.; Madura, J. D.; Impey, R. W.; Klein, M. L. *J. Chem. Phys.* **1983**, *79*, 926–35.
(62) Bayly, C.; Cieplak, P.; Cornell, W.; Kollman, P. J. *J. Phys. Chem.* **1993**, *97*, 10269–80.
(63) Wang, J.; Wolf, R. M.; Caldwell, J. W.; Kollman, P. A.; Case, D. A. *J. Comput. Chem.* **2004**, *25* (9), 1157–74.
(64) Genchev, G. Z.; Kallberg, M.; Gursoy, G.; Mittal, A.; Dubey, L.; Perisic, O.; Feng, G.; Langlois, R.; Lu, H. *Cell Biochem. Biophys.* **2009**, *55* (3), 141–52.
(65) Elber, R.; Karplus, M. *J. Am. Chem. Soc.* **1990**, *112* (25), 9161–75.
(66) Ludemann, S. K.; Lounnas, V.; Wade, R. C. *J. Mol. Biol.* **2000**, *303* (5), 797–811.
(67) Winn, P. J.; Ludemann, S. K.; Gauges, R.; Lounnas, V.; Wade, R. C. *Proc. Natl. Acad. Sci. U.S.A.* **2002**, *99* (8), 5361–6.
(68) Vashisth, H.; Abrams, C. F. *Biophys. J.* **2008**, *95* (9), 4193–204.
(69) Carlsson, P.; Burendahl, S.; Nilsson, L. *Biophys. J.* **2006**, *91* (9), 3151–61.
(70) Martinez, L.; Sonoda, M. T.; Webb, P.; Baxter, J. D.; Skaf, M. S.; Polikarpov, I. *Biophys. J.* **2005**, *89* (3), 2011–23.
(71) Martinez, L.; Webb, P.; Polikarpov, I.; Skaf, M. S. *J. Med. Chem.* **2006**, *49* (1), 23–6.

Table 1. Effect of Adjustable Parameters *f*, *N*, r_{min} on the Expulsion Rate and the Path Population Rate

f (kcal/mol · Å)	*N* (timesteps)	r_{min} (Å)	expulsion rate (%)	pw1/pw2 (%)
20	10	0.006	41	37/4
15	15	0.008	13	13/n.s[a]
10	20	0.008	3	3/n.s.

[a] n.s. stands for not sampled.

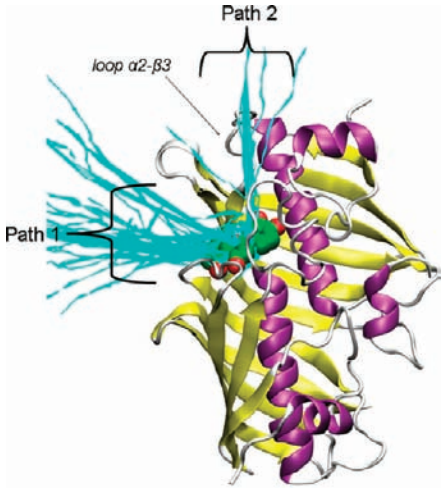

Figure 10. Unbinding trajectories generated by Random Acceleration Molecular Dynamics. The cyan segments represent the trails of the luteolin center of mass (carbon atoms in green spheres) escaping from the active site of *Pf*FabZ (purple, yellow, and white cartoons). The unbinding paths Path1 and Path2 are shown (see text for further details).

observed in the first 50 ps, then the run was stopped and considered unsuccessful. Preliminary investigations showed the ratio in the expulsion rate between Path1 and Path2 to be statistically independent from the binding mode of luteolin used as a starting configuration.

Vashisth and Abrams have recently implemented RAMD in NAMD via a *tcl* script interface,[68] which we modified to fit the needs of our system. The force was applied to all the carbon atoms of the molecule as well as to the intracyclic oxygen. The successful expulsion trajectories were clustered and the components of each cluster were then geometrically averaged to obtain the representative path. Two ligand exit pathways were identified (Figure 10): Path1, accounting for ligand escape through the most direct connection between the ligand and the protein surface; Path2, in which the ligand exploits an intrinsic conformational motion of *Pf*FabZ structure and flees between the flexible loop $\alpha2-\beta3$ and the central helix $\alpha2$.

The magnitude of the external force applied to the ligand largely influences the reliability of the escaping path. Therefore, a fine-tuning of simulation parameters is needed to sample physically relevant paths, which avoid improbable distortions of the receptor (see Table 1). Considering this, the occurrence of Path1 dominated the escaping trajectories regardless of the biasing force magnitude, while Path2 was sampled only a few times using the highest value of perturbing force. Its occurrence drastically dropped to zero for smaller forces (Table 1). Path2 was therefore not suited for the current study.

Path1 was thus selected as a reaction coordinate for the unbinding event and used to reconstruct the free-energy profile for the undocking of **12** and for the fast SMD simulations.

1.4. Potential of Mean Force Calculation. PMF along the unbinding reaction coordinate was reconstructed from unidirectional constant-velocity SMD pulling trajectories. Six independent trajectories, each 10 ns long, were generated for each binding mode (**12-A** and **12-B**). The value of the exerted force (f) was output every (dt) 1 ps of simulation and the work $W(t) = \int_0^t f(t')v dt'$ done on the system during the SMD was calculated by numerical integration; the pulling velocity (v) was 0.0005 Å ps^{-1}. The stiff spring approximation was satisfied by a spring constant of 7 kcal mol^{-1} Å^{-2}.

Although employing Jarzynski's equality[48] (eq 1) in theory allows the irreversible work to be discounted for any arbitrarily irreversible process,

$$e^{-\beta\Delta F} = \lim_{N\to\infty}\langle e^{-\beta W}\rangle_N \qquad \beta = 1/k_B T \tag{1}$$

in practice, its direct application is limited by the number of collectable trajectories as well as by the complexity of the biological system which often leads to a standard deviation (σ) of the work several times higher than $k_B T$.[25] Estimation of the exponential average $\langle e^{-\beta W}\rangle$ crucially depends on rarely sampled trajectories corresponding to the left tail of Gaussian work distribution.[25,44,47] On top of that, SMD pulling paths often sample the region around the peak rather than the tails of the Gaussian work distribution. As the spread of σ increases, the probability of sampling a region far from the peak decreases and the accuracy in reconstructing the potential of mean force is strongly biased. Such a systematic statistical uncertainty has been tackled in various ways in recent years, leading to more effective applications of the Jarzynski nonequilibrium work theorem.[45,47] The cumulant expansion approach up to second order (eq 2) has been widely applied[45,47,68,72] for reconstructing the free energy profile of biomolecular processes. It was here employed to compare the free energy profiles of configurations **12-A** and **12-B**.

$$\Delta F = \langle W\rangle - \frac{\sigma_W^2}{2k_B T} \qquad \sigma_W^2 = \langle W^2\rangle - \langle W\rangle^2 \tag{2}$$

Equation 2 directly suggests that free energy differences (ΔF) between states can be estimated by averaging the irreversible work $\langle W\rangle$ and discounting its variance σ_W^2. It follows that higher irreversible work trajectories are expected to have higher variance so that, in principle, one can obtain the same ΔF value employing eq 2 with different amounts of dissipated work (i.e., at different pulling velocities). As a consequence, the convergence of the estimates can be improved by reducing the dissipation (e.g., by merely diminishing the pulling velocity, or by introducing an artificial flow field which generates non-Hamiltonian trajectories).[73] Finally, the application of irreversible work obtained from forward and reverse SMD trajectories has emerged as a valuable way of providing accurate free energy estimates.[74,75] However, the bidirectional approach is not straightforwardly feasible in processes such as the undocking of a ligand from an enzyme in an explicitly solvated environment.

1.5. Force Profiling for Bioactivity Prediction. Comparison of the force profiles among different active and inactive flavonoids and for the prediction of rhamnetin (**23**) bioactivity was performed using constant-velocity SMD with a pulling rate of 0.025 Å ps^{-1} and with a spring constant of 7 kcal mol^{-1} Å^{-2}. Several pulling velocities were preliminarily tested. We chose the one that gave the best balance between resolution among different ligands and simulation time length. The time length of the simulations was 400 ps, which was sufficient to observe the complete ligand unbinding. The mean force profile for each ligand was obtained by averaging the outcomes of five independent runs. To avoid shifting of the system during pulling, the α-carbons of residues from Gly186 to Ile196 and from Leu207 to Asn214 on both chains A and B were

(72) Ytreberg, F. M. *J. Chem. Phys.* **2009**, *130* (16), 164906.
(73) Vaikuntanathan, S.; Jarzynski, C. *Phys. Rev. Lett.* **2008**, *100* (19), 190601.
(74) Chelli, R.; Procacci, P. *Phys. Chem. Chem. Phys.* **2009**, *11* (8), 1152–8.
(75) Forney, M. W.; Janosi, L.; Kosztin, I. *Phys. Rev. E: Stat., Nonlinear, Soft Matter Phys.* **2008**, *78* (5 Pt 1), 051913.

restrained to their initial position using a spring constant of 1 kcal mol^{-1} $Å^{-2}$. The starting configurations for the luteolin derivatives were obtained by superimposing the flavonoid scaffolds to **12-A**, and evolving the resulting ligand−protein complex for a further 3 ns. The number of water molecules was kept constant for both the luteolin binding mode investigation, and the flavonoids force profile comparison study.

2. Biological Assay. 2.1. Protein Purification and Inhibition Studies. Isolation and purification of *Pf*FabZ as well as subsequent inhibition studies with the flavonoid rhamnetin (**23**) were carried out as described previously by Tasdemir et al.[38]

Acknowledgment. The authors thank Matteo Masetti and Davide Branduardi at the Italian Institute of Technology for the inspiring and insightful discussions. We thank the CINECA Supercomputer Centre, Casalecchio di Reno (BO), Italy, for providing computer time. This research was supported by the University of Bologna.

Supporting Information Available: Stereoviews of configurations **12-A** and **12-B**. The ensemble of force profiles collected for PMF reconstruction. Tables and extended discussion on binding mode and SAR of flavonoid compounds. Complete refs 30, 52, and 56. This material is available free of charge via the Internet at http://pubs.acs.org.

JA100259R